PAPER

Check for updates

FTIR characterisation of chondroitin sulfate E (CS-E) di-, tetra-, and hexasaccharide derivatives and their biotinylated or reducing conjugates†

Elise Vincent, [a,b] Valérie Untereiner, [c] Florian Chabot, [d] Aude Vibert,[d] Marie Schuler, [d] Jorgan Guard, [a,b] Romain Rivet, [b] Isabelle Proult, [b] Chrystel Lopin-Bon, [d] Stéphane Brézillon *[b] and Ganesh D. Sockalingum *[a]

Sulfated glycosaminoglycans (GAGs), namely, chondroitin sulfate (CS), dermatan sulfate, keratan sulfate, heparin, and heparan sulfate, are linear complex polysaccharides that are covalently attached to core proteins to form proteoglycans. They are present at the cell surface and in the extracellular matrix and play a key role in the regulation of cellular microenvironmental effectors. To better understand the biological functions of GAGs and particularly of CS-E (4,6-disulfated) at the molecular level, structurally well-defined oligosaccharides are necessary. Chemically synthesised biotinylated conjugates are useful to study the interactions with proteins at the intra- and extracellular levels. Herein, FTIR spectroscopy was used to characterise nine chondroitin oligosaccharides, including biotinylated or reducing CS-E di-, tetra- and hexasaccharides as well as their non-sulfated analogs. Spectral features characteristic of the vibrational modes of oligosaccharides (1640, 1626, 1565, 1418, 1375, and 1160 cm^{-1}), CS-E (1280–1200, 1134, 1065, 1034, 1000, 927, and 866–860, 815 cm^{-1}), and biotin (1681, 1460, 1425, and 792 cm^{-1}) were identified. FTIR spectroscopy was sensitive enough to reveal structural microheterogeneity, allowing distinguishing C-4 from C-6 sulfated isoforms. CS-E- and biotin-specific signatures were obtained *via* difference spectra. PCA plots revealed three distinct groups: biotinylated oligosaccharides, CS-E biotinylated oligosaccharides and CS-E reducing oligosaccharides. Furthermore, the first component clearly distinguished sulfated from non-sulfated forms, while component two tended to discriminate according to the chain length, exclusively for non-sulfated oligosaccharides. Identifying the spectral signatures of these oligosaccharides is an important step for future research on the monitoring of the internalisation of oligosaccharide- and cell-penetrating peptide-bound forms in drug-delivery studies.

Introduction

Sulfated glycosaminoglycans (GAGs), namely, chondroitin sulfate (CS), dermatan sulfate, keratan sulfate, heparin, and heparan sulfate, are linear complex polysaccharides that are covalently attached to core proteins to form proteoglycans. They are mostly present at the cell surface and in the extra-cellular matrix (ECM).[1–3] The cell surface composition influences their cell internalisation. It has been reported that carbohydrates interact with cell-penetrating peptides (CPPs),[4,5] and penetratin has been shown to undergo a massive GAG-dependent entry into cells.[6–10] CPPs could self-assemble and were found to enter cells more efficiently, triggering a glycosaminoglycan-dependent pathway.[11–14] Santini and collaborators recently demonstrated that computationally designed cyclic peptides could effectively target GAGs, suggesting their potential as novel therapeutic agents.[15] It was also shown that GAGs, and in particular heparan sulfates, were able to selectively interact with proteins to control their internalisation.[16] Chondroitin sulfates are linear polysaccharides consisting of a disaccharide repeating unit composed of D-glucuronic acid (D-GlcA) and 2-acetamido-2-deoxy-D-galactose (D-GalNAc) arranged in the sequence [-4)-β-D-GlcA-(1-3)-β-D-GalNAc-(1-]$_n$ and bearing sulfate groups at various positions. The CS-sulfated units CS-D and CS-E are composed of the disaccharide

[a] Université de Reims Champagne-Ardenne, UR7506, BioSpecT, Reims, France. E-mail: ganesh.sockalingum@univ-reims.fr; Tel: +33 3 26 91 35 53

[b] Université de Reims Champagne-Ardenne, UMR CNRS/URCA n°7369, Matrice Extracellulaire et Dynamique Cellulaire (MEDyC), Laboratoire de Biochimie Médicale et Biologie Moléculaire, Reims, France. E-mail: stephane.brezillon@univ-reims.fr; Tel: +33 3 26 91 37 34

[c] Université de Reims Champagne-Ardenne, URCATech, PICT, Reims, France

[d] Institut de Chimie Organique et Analytique (ICOA), UMR 7311 CNRS et Université d'Orléans, BP 6759, Orléans cedex 02, France

†Electronic supplementary information (ESI) available. See DOI: https://doi.org/10.1039/d5an00136f

units GlcA2S-GalNAc6S and GlcA-GalNAc4S6S, respectively. The monosulfated units CS-A and CS-C consist of GlcA-GalNAc4S and GlcA-GalNAc6S disaccharide units, respectively. Highly sulfated CS subtypes are often linked to pathological conditions, including cancer.[17] CS-E plays an important role in numerous physiological and pathological processes.[18–21] Elevated expression of CS-E and CSPG (e.g., versican) in the ECM of ovarian cancer patients has been associated with poorer prognosis.[22–24] Vallen and collaborators demonstrated that CS-E is associated with metastatic lesions and that it confers tumors with adhesive properties.[25] In addition, chondroitin sulfate disaccharides have been reported as serum markers for primary serous epithelial ovarian cancer.[26–28] Furthermore, CS and its derivatives have been used as key components in drug- and gene-delivery systems due to their biocompatibility, low toxicity, and rapid biodegradability.[29,30] A more detailed overview of the biological structure/functions of CS was recently provided by Vijayakumar and collaborators.[18] In order to better understand the biological functions of GAGs at the molecular level, chemically synthesised and structurally well-defined CS-E (4,6-disulfated) and its biotinylated conjugates were suggested to be potentially useful tools.[31–34] Their characterisation is usually performed by classical analytical methods, such as NMR, HRMS and flash silica chromatography.[31–34]

In the present report, Fourier-transform infrared (FTIR) spectroscopy is proposed as an analytical tool to characterise a set of biotinylated or reducing di-, tetra-, and hexasaccharide chondroitin sulfate derivatives. FTIR is a rapid, reagent-free and non-destructive analytical tool that provides a molecular fingerprint of a sample. It has previously been used to characterise GAG standards.[35] The specific spectral signatures of polysaccharides and sulfates could be clearly identified by this method. Furthermore, the sulfation degree of the GAG standards could be assessed. FTIR spectroscopy was also sensitive enough to identify the structural microheterogeneities, enabling the distinction between chondroitin-4-sulfate and chondroitin-6-sulfate isoforms, wherein the sulfate group adopts an axial or equatorial orientation, respectively. FTIR spectroscopy has also been shown to be a useful tool to characterise GAGs in complex biological systems, such as single cells,[36–38] secretomes of cancer cells[36] and tissues.[37,39,40]

The main objective here was to determine whether FTIR spectroscopy could characterise a set of biotinylated or reducing synthetic di-, tetra-, and hexasaccharide derivatives with respect to the chain length, and presence or not of CS-, biotinylated or reducing forms.

Experimental

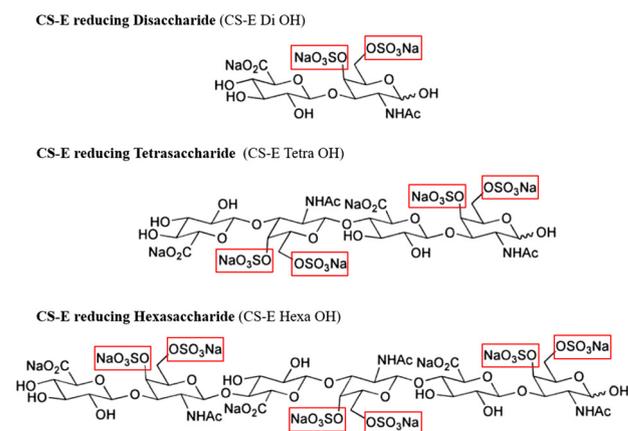### Chemical structures of the oligosaccharides

The synthesis of biotinylated and reducing CS-E oligosaccharides and their non-sulfated biotinylated analogs have already been reported.[32–34] Briefly, all these oligosaccharides can be obtained in 10–30 steps by an original and straightforward

process involving hemisynthesis from commercially available CS polymers,[31] which allows the gram-scale synthesis of a building block with suitable orthogonal protecting groups. Starting from this building block and following an efficient and stereo-controlled convergent strategy involving classical deprotection, deprotection, glycosylation and sulfation reactions, a library of reducing or biotinylated oligosaccharides of a defined-size (from di- to hexasaccharides) and defined-sulfation (CS-E or non-sulfated) patterns was obtained.

These oligosaccharides, including biotinylated or reducing CS-E di-, tetra- and hexasaccharides as well as non-sulfated analogs, were as follows: sulfated CS-E reducing disaccharide (CS-E Di OH), CS-E reducing tetrasaccharide (CS-E Tetra OH), CS-E reducing hexasaccharide (CS-E Hexa OH) (Fig. 1); sulfated CS-E biotinylated disaccharide (CS-E Di Biot), CS-E biotinylated tetrasaccharide (CS-E Tetra Biot), CS-E biotinylated hexasaccharide (CS-E Hexa Biot) (Fig. 2); non-sulfated biotinylated disaccharide (Di Biot), biotinylated tetrasaccharide (Tetra Biot) and biotinylated hexasaccharide (Hexa Biot) (Fig. 3).

### FTIR spectroscopy of the oligosaccharides and data analysis

All the oligosaccharides (Fig. 1–3) were obtained in lyophilised form after their synthesis (Institut de Chimie Organique et Analytique (ICOA), UMR 7311 CNRS et Université d'Orléans, France). They were solubilised in sterilised distilled water, and then one drop (5 μL) of each sample was deposited on an IR-transparent calcium fluoride (CaF$_2$) substrate and dried at room temperature. The FTIR spectra of the samples were recorded using the Spotlight 400 FTIR microscope coupled to a Frontier spectrometer (PerkinElmer, Villebon-sur-Yvette, France). For each sample, three to five spectra were recorded in transmission mode in the 4000–750 cm^{-1} spectral range, with an aperture size of 100 × 100 μm^2, using a 4 cm^{-1} spectral resolution and 128 accumulations. A reference spectrum on a clean surface of the CaF$_2$ substrate was acquired using the same parameters. This reference was automatically removed from the spectrum of the samples. All the spectra were aver-

Fig. 1 Chemical structures of the sulfated CS-E reducing di-, tetra-, and hexasaccharides. Red box indicates the position of the −OSO$_3$Na group.
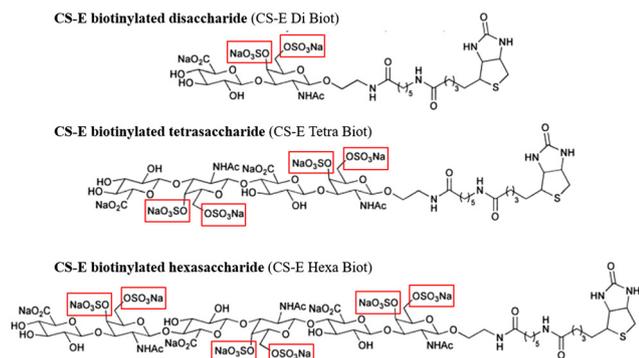
Fig. 2 Chemical structures of the sulfated CS-E biotinylated di-, tetra-, and hexasaccharides. Red box indicates the position of the −OSO$_3$Na group.
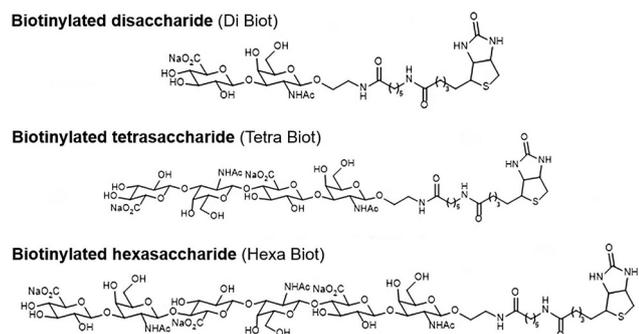
Fig. 3 Chemical structures of the non-sulfated biotinylated di-, tetra-, and hexasaccharides.

aged, baseline corrected using a rubber band method with 64 points, and vector normalised in the 1800–750 cm^{-1} spectral range prior to spectral comparison and calculation of the difference spectra. The difference spectra were computed with a subtraction coefficient of 1.

For chemometrics analysis, both hierarchical cluster analysis (HCA) and principal component analysis (PCA) were applied to the fingerprint region (1800–750 cm^{-1}) after vector normalisation.

Results and discussion

Dried-drop FTIR spectroscopy of the oligosaccharides

The mean FTIR spectral profiles of the chondroitin sulfate E di-, tetra-, and hexasaccharide derivatives and their biotinylated or reducing conjugates are displayed in Fig. 4.

Comparison of the nine mean spectra showed specific spectral features characteristic of oligosaccharide (1640, 1626, 1565, 1418, 1375, 1160 cm^{-1}), CS-E (1280–1200, 1134, 1065, 1034, 1000, 927, 866–860, 815 cm^{-1}), and biotin (1681, 1460, 1425, 792 cm^{-1}) vibrational modes (Fig. 4).
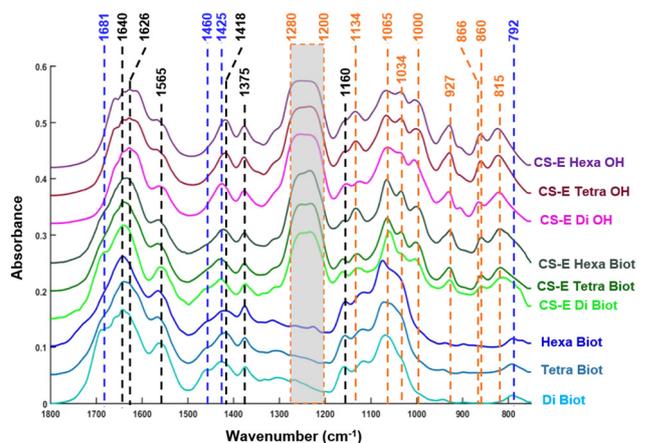
Fig. 4 Mean FTIR profiles of chondroitin sulfate E di-, tetra-, and hexasaccharide derivatives and their biotinylated or reducing conjugates. Assignment of specific peaks to biotin (blue dashed line), CS-E (orange dashed line) and oligosaccharides (black dashed line) molecular structures.

In addition, FTIR spectroscopy was sensitive enough to identify the structural microheterogeneity allowing distinguishing C-4 (927 and 866–860 cm^{-1}) from C-6 (1000 and 815 cm^{-1}) sulfated isoforms, as previously found.[35] The powerful sensitivity of FTIR spectroscopy is promising in the perspective of being able to detect C6S-derived oligosaccharides cancer biomarkers.[17,21,25]

In order to confirm these assignments, difference spectra were calculated. CS-E-specific signatures were obtained by subtracting the biotinylated oligosaccharides from their corresponding CS-E forms (Fig. 5). Hence, the difference spectra exhibited CS-E specific peaks at 1280–1200 cm^{-1} (asymmetric
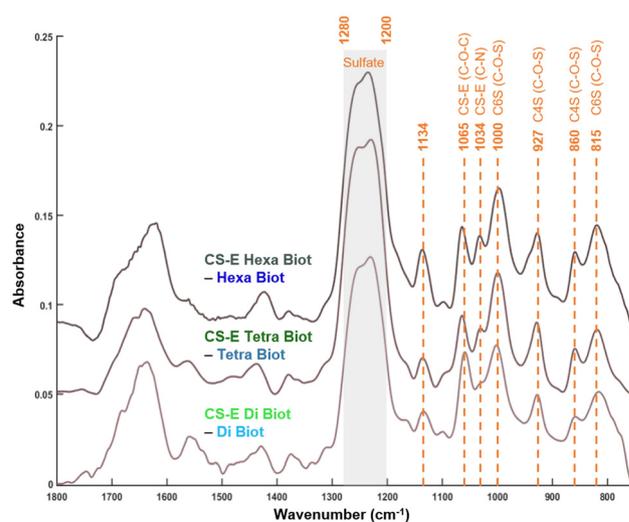
Fig. 5 Difference spectra obtained by subtracting non-sulfated biotinylated forms from their corresponding CS-E analogs (subtraction coefficient of 1). Assignment of specific peaks associated with CS-E vibrational modes (orange dashed line).

SO_4^{2-}), 1134, 1065 cm^{-1} (C–O–C/symmetric SO_4^{2-}), 1034 cm^{-1} (C–N), 1000 cm^{-1} (C–O–S from C6S), 927 cm^{-1} (C–O–S from C4S), 860 cm^{-1} (C–O–S from C4S), 815 cm^{-1} (C–O–S from C6S), allowing differentiation between the two isoforms. It is known that the CS-E structure contains two sulfate groups, one in the C-4 and the other in the C-6 position. Therefore, in our data, information of the sulfate groups from both the C-4 and C-6 positions were present and could be identified in both Fig. 4 and 5.

Similarly, biotin-specific signatures were obtained by subtracting the reducing forms from their corresponding biotinylated analogs (Fig. 6). The results showed that biotin-specific signatures could be associated with the peaks at 1681 cm^{-1} (C=O vibration), 1460 cm^{-1} (CH$_2$ deformation), 1425 cm^{-1} (O–H deformation), and 792 cm^{-1} (C–H twist). These main specific signatures and their tentative assignments were done based on published data,[35,38,41,42] and are summarised in Table 1.

Chemometrics analysis

In order to better appraise the spectral differences between the sulfated CS-E reducing oligosaccharides, sulfated CS-E biotinylated oligosaccharides, and non-sulfated biotinylated oligosaccharides, unsupervised chemometrics analysis was performed using HCA and PCA on the vector-normalised mean spectra in the 1800–750 cm^{-1} spectral region. Fig. 7A shows the resulting dendrogram. At first glance, it shows a clear separation between the sulfated and non-sulfated oligosaccharides. In

Table 1 Tentative assignments of specific peaks (reducing, biotinylated and CS-E forms) observed in the FTIR spectra of the nine oligosaccharides. def: deformation. These main specific signatures and their tentative assignments are achieved based on published data[35,38,41,42]

Wavenumber (cm^{-1})	Tentative assignment
1681	C=O (biotin)
1640	C=O (–CONH) (oligosaccharides)
1565	N–H def (oligosaccharides)
1460	CH$_2$ def (biotin)
1425	O–H def (biotin)
1375	C–C (oligosaccharides)
1280–1200	Asymmetric SO_4^{2-} (CS-E)
1160	C–O–C (saccharide)
1065	Symmetric SO_4^{2-}, C–O–C (CS-E)
1034	C–N (CS-E)
1000	C–O–S in equatorial position CS-E (C6S)
927	C–O–S, CS-E (C4S)
866–860	C–O–S in axial position CS-E (C4S)
815	C–O–S in equatorial position CS-E (C6S)
792	C–H twist (biotin)

addition, within the CS-E oligosaccharides, a good discrimination between the biotinylated and reducing forms was found. This analysis shows the stronger impact of the sulfate groups on this classification compared to the presence of the biotin moiety. However, this classification does not indicate any tendency for the chain length except for the non-sulfated oligosaccharides.

The data were further analysed using principal component analysis (PCA) to confirm the previous results and to gain more insights into the structural characteristics of these oligosaccharides. Fig. 7B displays the score plot using the principal components 1 and 2 (accounting for 90.9% of the total variance) after data mean centering. This analysis confirmed the results obtained above using HCA with a clear-cut difference between the different types: sulfated CS-E reducing oligosaccharides, sulfated CS-E biotinylated oligosaccharides, and non-sulfated biotinylated oligosaccharides.

The first principal component (PC1) distinguished the sulfated from the non-sulfated forms. This was confirmed by the profile of PC1 (Fig. 7C), where the sulfate bands between 1234 and 1256 cm^{-1} (asymmetric SO_4^{2-}) and C–O–S vibrations at 999, 929, 860 and 822 cm^{-1} were more pronounced. In addition, PC2 showed major contributions from the peaks at 1692, 1651, 1536, 1060 and 788–779 cm^{-1}, which may be attributed to biotin signatures. The other peaks present could be assigned to repeating disaccharide units. PC2 also tended to discriminate according to the chain length of the oligosaccharides exclusively for the non-sulfated oligosaccharides. A possible explanation for this is that the presence of the CS-E component carried a higher variance, thus compromising the effect of the chain length.

In addition, it could be observed that the reducing CS-E (non-biotinylated) cluster showed a lower intra variability (red symbols), while the presence of biotin tended to enhance the variability within the groups (green and blue symbols). Generally, GAG-derived oligosaccharides are analysed by NMR,
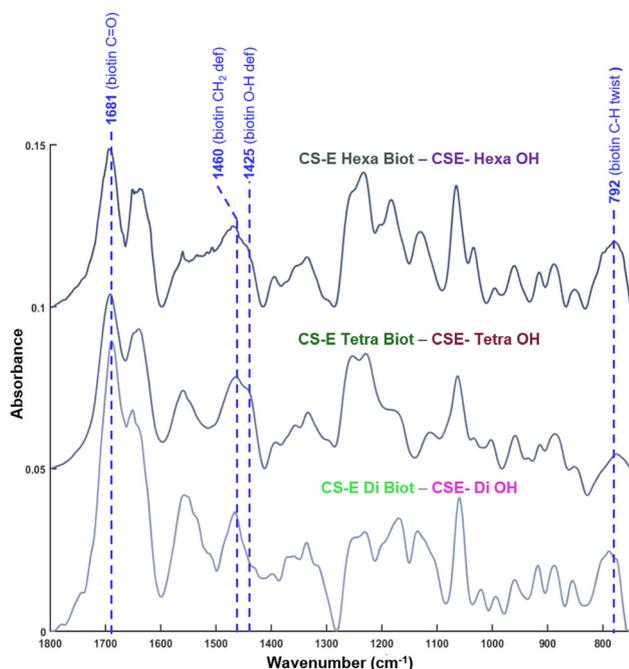
Fig. 6 Difference spectra obtained by subtracting reducing forms from their corresponding biotinylated analogs (subtraction coefficient of 1). Assignment of specific peaks associated with biotin vibrational modes (blue dashed line).
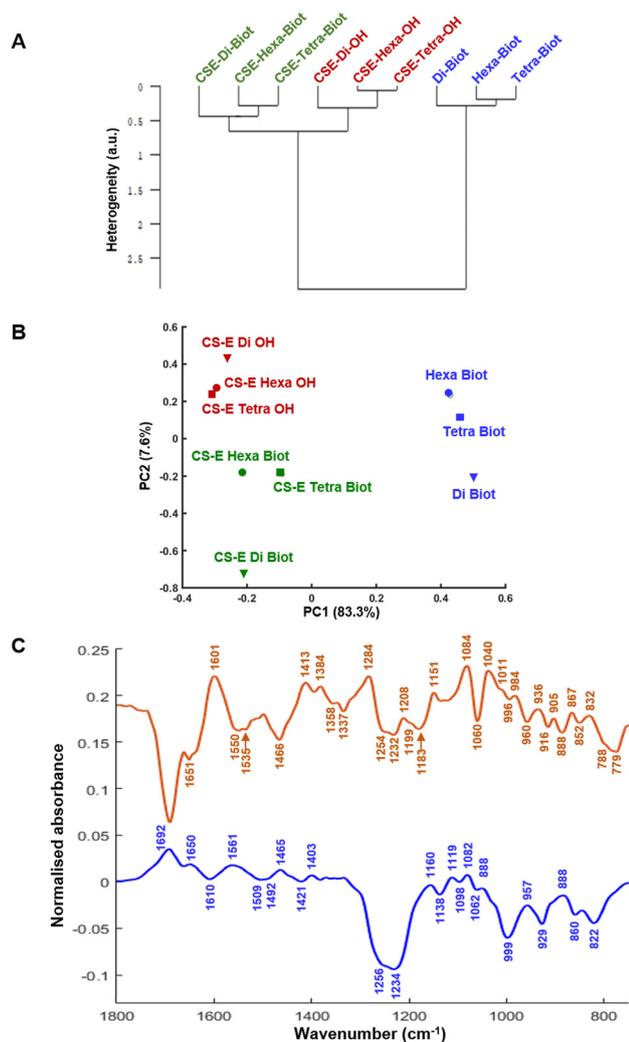
Fig. 7 Chemometric analysis of the mean normalised spectra of the nine oligosaccharides using the 1800–750 cm^{-1} spectral range. (A) Dendrogram showing the clustering of the nine oligosaccharides. (B) Principal component analysis using the scores of PC1 and PC2. Triangle, square and circle indicate di-, tetra- and hexasaccharides, respectively. Biotinylated oligosaccharides (blue color), CS-E biotinylated oligosaccharides (green color) and CS-E reducing oligosaccharides (red color). (C) Loading vectors corresponding to PC1 (orange curve) and PC2 (blue curve).

HRMS, flash silica chromatography or by HPLC with fluorescence detection.[31–34,43] However, we show here that FTIR spectroscopy could provide, in a direct, non-destructive, and reagent-free manner, characteristic information on the CS-E oligosaccharide derivatives as well as their biotinylated or reducing conjugates.

GAGs have been shown to be implicated in the endocytosis of several CPPs. CPPs are considered to be promising systems for the intracellular delivery of molecular probes and therapeutic drugs. They are generally short purely basic or amphipathic peptides that can enter cells by two different pathways: endocytosis and direct translocation across the plasma membrane. Several CPPs are currently under clinical development.

CPP arginine residues play an essential role in GAG binding, due to their ability to form bidentate hydrogen bonds with GAG carboxylate and sulfate groups.[11] For instance, the internalization mechanism of Engrailed2 (En2), a cationic protein that is a transcription factor, is proposed to require an initial interaction with GAGs on the cell surface.[16] This study demonstrated the critical role of GAGs as an entry gate, finely tuning the homeoprotein capacity to internalise into cells. Using glycan microarray analysis, the CPP En2 was shown to preferentially bind to long and highly sulfated HS oligosaccharides. The presence of soluble CS-E in the ECM was shown to either promote or inhibit En2 internalisation in CHO-K1 cells, depending on the GAG concentration, as observed with soluble heparin. These data suggest that membrane surface CS-E could also play a role in CPP internalisation.[16]

Our preliminary results on pgsA-745 cell lysates spiked with different amounts of chondroitin sulfate E showed that FTIR spectroscopy was capable of detecting as low as 5 μg of chondroitin sulfate in the cell lysate at a protein concentration of 1 μg μL^{-1} (see ESI Fig. 1†). The same detection limit was obtained with a protein concentration of 0.1 μg μL^{-1} (data not shown). The pgsA-745 cell line was chosen since it is a mutant of the CHO-K1 cell line, with the characteristics of being deficient in xylosyltransferase, so it consequently produces a very low amount of glycosaminoglycans in comparison with the wild-type CHO-K1 cell line. In this sense, there was no overlapping with the spectral signatures of the spiked chondroitin sulfate.

Conclusions

FTIR spectroscopy analysis of nine synthesised biotinylated or reducing CS-E oligosaccharides and their non-sulfated biotinylated analogs provided specific spectral signatures that could be attributed to the oligosaccharides, CS-E forms and biotin. FTIR could further identify microheterogeneities within the isoforms, allowing differentiating C4-S from C6-S. HCA and PCA unsupervised analyses objectively allowed differentiating the three different groups of samples, separating the sulfated forms from the biotinylated ones. These characteristic signatures could be identified in the loading vectors obtained from PCA analysis. Further, the effect of the chain length could also be detected in the PCA plot, albeit exclusively for the non-sulfated oligosaccharides.

These results are interesting and promising in view of a better understanding of the molecular and structural properties of these molecules. Indeed, identifying the spectral signatures of these oligosaccharides is an important step for future research into the monitoring of the internalisation of the oligosaccharides and CPP-bound forms in drug-delivery studies.

Author contributions

EV: investigation, methodology and editing. VU: investigation, writing, reviewing and editing. FC: investigation and method-

Data availability

The data that support the findings of this study are available from the corresponding author upon reasonable request.

Conflicts of interest

There are no conflicts to declare.

Acknowledgements

References

1 S. Ricard-Blum, R. R. Vivès, L. Schaefer, et al., A biological guide to glycosaminoglycans: current perspectives and pending questions, FEBS J., 2024, 291(15), 3331–3366, DOI: 10.1111/febs.17107.

2 S. D. Vallet, C. Berthollier and S. Ricard-Blum, The glycosaminoglycan interactome 2.0, Am. J. Physiol.: Cell Physiol., 2022, 322(6), C1271–C1278, DOI: 10.1152/ajpcell.00095.2022.

3 J. Oto, Q. K. Le, S. D. Schäfer, et al., Role of Syndecans in Ovarian Cancer: New Diagnostic and Prognostic Biomarkers and Potential Therapeutic Targets, Cancers, 2023, 15(12), 3125, DOI: 10.3390/cancers15123125.

4 E. Dupont, A. Prochiantz and A. Joliot, Penetratin Story: An Overview, Methods Mol. Biol., 2015, 1324, 29–37, DOI: 10.1007/978-1-4939-2806-4_2.

5 C. Rampon, C. Gauron, T. Lin, et al., Control of brain patterning by Engrailed paracrine transfer: a new function of the Pbx interaction domain, Development, 2015, 142(10), 1840–1849, DOI: 10.1242/dev.114181.

6 I. D. Alves, C. Bechara, A. Walrant, Y. Zaltsman, C. Y. Jiao and S. Sagan, Relationships between membrane binding, affinity and cell internalization efficacy of a cell-penetrating peptide: penetratin as a case study, PLoS One, 2011, 6(9), e24096, DOI: 10.1371/journal.pone.0024096.

7 A. Walrant, A. Bauzá, C. Girardet, et al., Ionpair-π interactions favor cell penetration of arginine/tryptophan-rich cell-penetrating peptides, Biochim. Biophys. Acta, Biomembr., 2020, 1862(2), 183098, DOI: 10.1016/j.bbamem.2019.183098.

8 A. Walrant, C. Bechara, I. D. Alves and S. Sagan, Molecular partners for interaction and cell internalization of cell-penetrating peptides: how identical are they?, Nanomedicine, 2012, 7(1), 133–143, DOI: 10.2217/nnm.11.165.

9 A. Walrant, S. Cardon, F. Burlina and S. Sagan, Membrane Crossing and Membranotropic Activity of Cell-Penetrating Peptides: Dangerous Liaisons?, Acc. Chem. Res., 2017, 50(12), 2968–2975, DOI: 10.1021/acs.accounts.7b00455.

10 A. Walrant, I. Correia, C. Y. Jiao, et al., Different membrane behaviour and cellular uptake of three basic arginine-rich peptides, Biochim. Biophys. Acta, 2011, 1808(1), 382–393, DOI: 10.1016/j.bbamem.2010.09.009.

11 M. Amoura, F. Illien, A. Joliot, et al., Head to tail cyclisation of cell-penetrating peptides: impact on GAG-dependent internalisation and direct translocation, Chem. Commun., 2019, 55(31), 4566–4569, DOI: 10.1039/c9cc01265f.

12 C. Bechara, M. Pallerla, Y. Zaltsman, et al., Tryptophan within basic peptide sequences triggers glycosaminoglycan-dependent endocytosis, FASEB J., 2013, 27(2), 738–749, DOI: 10.1096/fj.12-216176.

13 C. Bechara, M. Pallerla, F. Burlina, F. Illien, S. Cribier and S. Sagan, Massive glycosaminoglycan-dependent entry of Trp-containing cell-penetrating peptides induced by exogenous sphingomyelinase or cholesterol depletion, Cell. Mol. Life Sci., 2015, 72(4), 809–820, DOI: 10.1007/s00018-014-1696-y.

14 S. A. Bode, M. Thévenin, C. Bechara, et al., Self-assembling mini cell-penetrating peptides enter by both direct translocation and glycosaminoglycan-dependent endocytosis, Chem. Commun., 2012, 48(57), 7179–7181, DOI: 10.1039/c2cc33240j.

15 B. L. Santini, M. Gaardløs, D. Wyrzykowski, et al., Rational design of glycosaminoglycan binding cyclic peptides using cPEPmatch, Comput. Struct. Biotechnol. J., 2024, 23, 2985–2994, DOI: 10.1016/j.csbj.2024.07.016.

16 S. Cardon, Y. P. Hervis, G. Bolbach, et al., A cationic motif upstream Engrailed2 homeodomain controls cell internalization through selective interaction with heparan sulfates,

Nat. Commun., 2023, **14**(1), 1998, DOI: 10.1038/s41467-023-37757-6.

17 A. Pudełko, G. Wisowski, K. Olczyk and E. M. Koźma, The dual role of the glycosaminoglycan chondroitin-6-sulfate in the development, progression and metastasis of cancer, *FEBS J.*, 2019, **286**(10), 1815–1837, DOI: 10.1111/febs.14748.

18 S. Vijayakumar, Z. I. González-Sánchez, M. Divya, M. Amanullah, E. F. Durán-Lara and M. Li, Efficacy of chondroitin sulfate as an emerging biomaterial for cancer-targeted drug delivery: A short review, *Int. J. Biol. Macromol.*, 2024, **283**(Pt 2), 137704, DOI: 10.1016/j.ijbiomac.2024.137704.

19 J. Yang, M. Shen, H. Wen, *et al.*, Recent advance in delivery system and tissue engineering applications of chondroitin sulfate, *Carbohydr. Polym.*, 2020, **230**, 115650, DOI: 10.1016/j.carbpol.2019.115650.

20 A. Hossain, D. Dave and F. Shahidi, Sulfated polysaccharides in sea cucumbers and their biological properties: A review, *Int. J. Biol. Macromol.*, 2023, **253**(Pt 7), 127329, DOI: 10.1016/j.ijbiomac.2023.127329.

21 J. Iida, J. Dorchak, R. Clancy, *et al.*, Role for chondroitin sulfate glycosaminoglycan in NEDD9-mediated breast cancer cell growth, *Exp. Cell Res.*, 2015, **330**(2), 358–370, DOI: 10.1016/j.yexcr.2014.11.002.

22 S. C. H. A. van der Steen, A. A. G. van Tilborg, M. J. E. Vallen, J. Bulten, T. H. van Kuppevelt and L. F. A. G. Massuger, Prognostic significance of highly sulfated chondroitin sulfates in ovarian cancer defined by the single chain antibody GD3A11, *Gynecol. Oncol.*, 2016, **140**(3), 527–536, DOI: 10.1016/j.ygyno.2015.12.024.

23 M. C. Vos, E. Hollemans, N. Ezendam, *et al.*, MMP-14 and CD44 in Epithelial-to-Mesenchymal Transition (EMT) in ovarian cancer, *J. Ovarian Res.*, 2016, **9**(1), 53, DOI: 10.1186/s13048-016-0262-7.

24 M. C. Vos, E. Hollemans, S. C. H. A. van der Steen, T. H. van Kuppevelt, A. A. M. van der Wurff and L. F. A. G. Massuger, Primary Ovarian Tumors With Lymphogenic and Hematogenic Metastasis Express High MMP-14, Which Colocalizes With Highly Sulfated Chondroitin Sulfate in the Stroma, *Int. J. Gynecol. Pathol.*, 2020, **39**(2), 184–192, DOI: 10.1097/PGP.0000000000000587.

25 M. J. E. Vallen, S. Schmidt, A. Oosterhof, J. Bulten, L. F. A. G. Massuger and T. H. Van Kuppevelt, Primary Ovarian Carcinomas and Abdominal Metastasis Contain 4,6-Disulfated Chondroitin Sulfate Rich Regions, Which Provide Adhesive Properties to Tumour Cells. Karamanos NK, ed, *PLoS One*, 2014, **9**(11), e111806, DOI: 10.1371/journal.pone.0111806.

26 G. B. ten Dam, E. M. A. van de Westerlo, A. Purushothaman, *et al.*, Antibody GD3G7 selected against embryonic glycosaminoglycans defines chondroitin sulfate-E domains highly up-regulated in ovarian cancer and involved in vascular endothelial growth factor binding, *Am. J. Pathol.*, 2007, **171**(4), 1324–1333, DOI: 10.2353/ajpath.2007.070111.

27 M. J. E. Vallen, L. F. A. G. Massuger, G. B. ten Dam, J. Bulten and T. H. van Kuppevelt, Highly sulfated chondroitin sulfates, a novel class of prognostic biomarkers in ovarian cancer tissue, *Gynecol. Oncol.*, 2012, **127**(1), 202–209, DOI: 10.1016/j.ygyno.2012.06.022.

28 K. Biskup, C. Stellmach, E. I. Braicu, J. Sehouli and V. Blanchard, Chondroitin Sulfate Disaccharides, a Serum Marker for Primary Serous Epithelial Ovarian Cancer, *Diagnostics*, 2021, **11**(7), 1143, DOI: 10.3390/diagnostics11071143.

29 Y. Ji, S. Zhang, M. Qiao, *et al.*, Synthesis of structurally defined chondroitin sulfate: Paving the way to the structure-activity relationship studies, *Carbohydr. Polym.*, 2020, **248**, 116796, DOI: 10.1016/j.carbpol.2020.116796.

30 S. Morla, O. Ravikumar, C. O'Hara, *et al.*, Designing Synthetic, Sulfated Glycosaminoglycan Mimetics That Are Orally Bioavailable and Exhibiting In Vivo Anticancer Activity, *J. Med. Chem.*, 2023, **66**(2), 1321–1338, DOI: 10.1021/acs.jmedchem.2c01511.

31 C. Lopin and J. C. Jacquinet, From polymer to size-defined oligomers: an expeditious route for the preparation of chondroitin oligosaccharides, *Angew. Chem., Int. Ed.*, 2006, **45**(16), 2574–2578, DOI: 10.1002/anie.200503551.

32 A. Vibert, C. Lopin-Bon and J. C. Jacquinet, From polymer to size-defined oligomers: a step economy process for the efficient and stereocontrolled construction of chondroitin oligosaccharides and biotinylated conjugates thereof: part 1, *Chemistry*, 2009, **15**(37), 9561–9578, DOI: 10.1002/chem.200900740.

33 J. C. Jacquinet, C. Lopin-Bon and A. Vibert, From polymer to size-defined oligomers: a highly divergent and stereo-controlled construction of chondroitin sulfate A, C, D, E, K, L, and M oligomers from a single precursor: part 2, *Chemistry*, 2009, **15**(37), 9579–9595, DOI: 10.1002/chem.200900741.

34 J. C. Jacquinet and C. Lopin-Bon, Stereocontrolled preparation of biotinylated chondroitin sulfate E di-, tetra-, and hexasaccharide conjugates, *Carbohydr. Res.*, 2015, **402**, 35–43, DOI: 10.1016/j.carres.2014.09.007.

35 N. Mainreck, S. Brézillon, G. D. Sockalingum, F. X. Maquart, M. Manfait and Y. Wegrowski, Rapid characterization of glycosaminoglycans using a combined approach by infrared and Raman microspectroscopies, *J. Pharm. Sci.*, 2011, **100**(2), 441–450, DOI: 10.1002/jps.22288.

36 H. T. Mohamed, V. Untereiner, G. D. Sockalingum and S. Brézillon, Implementation of infrared and Raman modalities for glycosaminoglycan characterization in complex systems, *Glycoconjugate J.*, 2017, **34**(3), 309–323, DOI: 10.1007/s10719-016-9743-6.

37 H. T. Mohamed, V. Untereiner, I. Proult, *et al.*, Characterization of inflammatory breast cancer: a vibrational microspectroscopy and imaging approach at the cellular and tissue level, *Analyst*, 2018, **143**(24), 6103–6112, DOI: 10.1039/c8an01292j.

38 S. Brézillon, V. Untereiner, L. Lovergne, *et al.*, Glycosaminoglycan profiling in different cell types

using infrared spectroscopy and imaging, *Anal. Bioanal. Chem.*, 2014, **406**(24), 5795–5803, DOI: **10.1007/s00216-014-7994-2**.

39 P. Nizet, V. Untereiner, G. D. Sockalingum, *et al.*, Assessment of Ovarian Tumor Growth in Wild-Type and Lumican-Deficient Mice: Insights Using Infrared Spectral Imaging, Histopathology, and Immunohistochemistry, *Cancers*, 2021, **13**(23), 5950, DOI: **10.3390/cancers13235950**.

40 L. Nannan, V. Untereiner, I. Proult, *et al.*, Label-Free Infrared Spectral Histology of Skin Tissue Part I: Impact of Lumican on Extracellular Matrix Integrity, *Front. Cell Dev. Biol.*, 2020, **8**, 320, DOI: **10.3389/fcell.2020.00320**.

41 M. Emami, A. Teimouri and A. N. Chermahini, Vibrational spectra and assignments using ab initio and density func- tional theory analysis on the structure of biotin, *Spectrochim. Acta, Part A*, 2008, **71**(4), 1516–1524, DOI: **10.1016/j.saa.2008.05.020**.

42 V. Balan, I. A. Petrache, M. I. Popa, *et al.*, Biotinylated chito- san-based SPIONs with potential in blood-contacting appli- cations, *J. Nanopart. Res.*, 2012, **14**(2), 730, DOI: **10.1007/s11051-012-0730-y**.

43 T. Ishii, K. Hirai, K. Higashi, *et al.*, Novel simultaneous analysis of 18 types of glycosaminoglycan-derived disacchar- ides using 4-aminobenzoic acid ethyl ester derivatization by HPLC with fluorescence detection, *Anal. Bioanal. Chem.*, 2024, **416**(28), 6209–6221, DOI: **10.1007/s00216-024-05504-5**.